Guest−Host Colloid Crystals: Experimental Study and Simulations

Chantal Paquet, Mathieu Allard,† Grégory Glédel, and Eugenia Kumacheva*

Department of Chemistry, University of Toronto, Toronto, Ontario, Canada

Received: April 6, 2005; In Final Form: September 7, 2005

Disorder in colloid crystals was induced by doping them with a different number of large or small guest particles, which had a different deviation in size from the host colloids. The change in optical properties of the guest−host colloid crystals was assessed by using optical transmission spectroscopy while the variation in crystal structure was examined using scanning electron microscopy (SEM). The disruption in the crystalline lattices depended on the relative deviation in sizes of the guest and host particles and the concentration of the guest colloids. In parallel with experiments, the packing of spheres in guest−host crystals was modeled with a simulated annealing algorithm. A good correlation was found between the changes in crystal structure observed by SEM imaging and the simulated sphere packing. The experimental and simulated changes in the transmission spectra of guest−host colloid crystals were in good agreement.

Introduction

The self-assembly of submicrometer-sized particles into colloid crystals (CCs) is a general bottom-up approach to fabricating photonic crystals. Photonic crystals possess a spatial periodicity on the length scale of the colloid building block, which causes coherent interference of light with wavelengths commensurate with the sphere size. The coherent interference caused by multiple scattering by the crystal planes forbids light from propagating in certain directions depending on the symmetry and the refractive index of the colloid crystal. The range of wavelengths over which propagation of light is forbidden (the stopband) manifests itself as a dip in the transmission spectrum. Photonic crystals have been proposed as the foundation for devices such as waveguides, tunable wavelength filters, and limiters.[1−3] These devices, however, require nearly perfect crystal lattices. To overcome difficulties in producing large single crystals or crystals with minor defects, extensive research has focused on enhancing the extent of order in CCs by optimizing methods of their fabrication.

Several approaches to fabricating self-assembled CCs include crystallization by sedimentation,[4] spin-coating,[5] and deposition of colloids on a prepatterned surface[6,7] and crystallization under confinement,[8−11] oscillatory shear,[12] and the action of electric and magnetic fields.[13−15] A well-established approach to CCs is the convective self-assembly of colloid particles on planar surfaces.[16] In this approach, crystallization of microspheres into a close-packed array occurs through attractive capillary forces acting between the beads.[17] This method yields large-area CCs with a relatively low density of defects.

Typical defects in large-area colloid crystals obtained by self-assembly or assisted assembly techniques include grain boundaries, stacking faults, vacancies, and dislocations. The formation of defects is influenced by the crystallization conditions such as temperature, relative humidity, ionic strength, concentration of colloid particles, and the properties of the dispersion medium.[17−21] An important factor controlling the density of defects is the distribution of sizes of colloid particles: as the distribution of microsphere sizes broadens, a highly ordered lattice transforms into a completely disordered structure. Several studies have acknowledged that a coefficient of variation in particle size greater than ca. 8% is detrimental to the quality of colloid crystals.[16,22,23] Yet, the mechanism by which the structure of the CC is disrupted by polydispersity of the building blocks remains unclear.

Disorder affects the optical properties of colloid crystals in several ways. When the amount of disorder increases, the transmission increases in the stopband *and* decreases outside the stopband:[24−30] coherent scattering off the Bragg planes is gradually replaced by incoherent scattering off crystal defects. In addition, disorder leads to broadening of the width of the stopband and decreasing transmission outside the stopband.[29,31]

Most of studies that elucidated the relationship between particle polydispersity and the properties of CCs have been theoretical; they used simplified models of disorder in arrays. For instance, disorder in lattices of two-dimensional cylinders was modeled by introducing deviations in the diameter of the cylinders and in their displacement from their respective lattice sites.[32] Simulations of the optical transmission of the array of cylinders showed a thresholdlike behavior: a minimal deviation of 10−15% in the size of cylinders was required for a significant increase in light transmission in the stopband. In another study, disorder was modeled for a close-packed lattice of spheres possessing small deviations in diameter.[25] In this study, the attenuation calculated for the stopband was significantly stronger than that measured in real CCs. Strong attenuation in the stopband predicted by the models of disordered CCs occurred most probably because the model underestimated the extent of the total disruption of the lattice caused by polydispersity.

This shortcoming has been recently addressed by a new model that accounted for the global reorganization of the lattice caused by deviations in the size of the particles. Allard and Sargent devised a model that simulated the assembly of a collection of spheres with a given size distribution and predicted a transition from an ordered to a disordered arrangement of the spheres when their polydispersity (measured as the standard deviation of the

* To whom correspondence should be addressed. E-mail: ekumache@chem.utoronto.ca.

† Hospital for Sick Children, Toronto, Ontario, Canada.

10.1021/jp051783j CCC: $33.50
Published on Web 01/05/2006

distribution) reached a value between 3 and 4%.[33] Simulations of the optical properties of the arrays of spheres showed that this transition was accompanied by a significant increase in the transmission in the stopband. The output of modeling was validated by experimental results.

Experimental studies of the effect of polydispersity of colloid particles on the structure and optical properties of CCs have been conducted by Gates and Xia.[24] In this work, CCs were doped with small guest particles; increasing the density of guest particles led to an increasing density of defects (that is, decreasing size of single domains) and to a monotonic increase in transmission in the stopband. Recently, Colvin et al have explored the relationship between the size distribution of colloids and the structural and optical properties of CCs.[23] The authors found that the structural and optical properties of CCs significantly degraded when the colloids possessed a polydispersity of 6%.

Herein, we report a comprehensive study of the role of polydispersity of colloid particles on the structure and optical properties of colloid crystals. We fabricated CCs from dispersions of two populations of monodispersed colloids with different average sizes. Adjusting the relative concentration of the two populations of particles in the dispersion allowed for the control of the overall spread in the size distribution of the particles. The relevance of this system was enhanced by the fact that bimodal size distribution of microbeads represents a frequently encountered size distribution of polymer or silica microbeads, which results from secondary nucleation or coalescence during synthesis of colloid dispersions.[34,35]

We found significant differences in the structure and optical properties of CCs fabricated from guest−host particles with a different size ratio and concentration. For instance, for the same absolute deviation in sizes between the guest and host microspheres, smaller guest particles had less impact on the disorder and optical properties than larger guest particles. In addition, guest particles with large absolute size deviations from the host showed a greater impact on the structure and the optical properties of the CCs than the microspheres with smaller absolute size deviation. We also simulated the assembly and transmission spectra of these binary colloid dispersions by using the approach of Allard and Sargent.[33] The simulations revealed the ability of host particles to form cage structures around small guest particles, without impacting neighboring lattice sites. By contrast, the lattice did not accommodate larger guest particles, which caused a long-range disturbance. Overall, good agreement was obtained in the simulations and experimental study of the changes in the crystal structure and optical properties of guest−host colloid crystals.

Experimental Section

Materials. The monomer, methyl methacrylate (MMA), cross-linking agent, ethylene glycol dimethacrylate (EGDMA), chain transfer agent, 1-dodecanthiol, and initiator, ammonium persulfate ($[NH_4]_2S_2O_8$) were purchased from Aldrich Canada and used without further purification. Ultrapure water (18.2 MΩ cm^{-1}) was supplied by a Milli-Q water purification system. Microslides (3 in. × 1 in. × 1 mm, Corning) were cut into quarters and used as substrates. Glass scintillation vials (20 mL) were used as cells for CC growth.

Synthesis of Colloid Particles. Poly(methyl methacrylate) (PMMA) particles were synthesized by emulsion surfactant-free polymerization.[36] Particles with a diameter of 295 nm were synthesized under batch conditions. Prior to polymerization, 0.20 g of $[NH_4]_2S_2O_8$ and 90.0 g of Milli-Q water were precharged in the reaction flask and stirred for ca. 1 h until the mixture reached 80 ± 0.1 °C. At this temperature, a mixture of 10.00 g of MMA, 0.10 g of EGDMA, and 0.04 g of 1-dodecanethiol was added to the reactor. The polymerization reaction was carried out for 3 h. Particles with diameters of 319, 389, 271, and 202 nm were prepared in the same manner; however, the amount of MMA or the volume ratio of MMA/water was varied. The weight fraction of particles in the dispersions was determined by weighing a small aliquot of the dispersion before and after drying. The number of particles with a particular size in each dispersion was determined by dividing their total weight in dispersion by the weight of a single particle (using the density for PMMA of 1.18 g/cm^3).

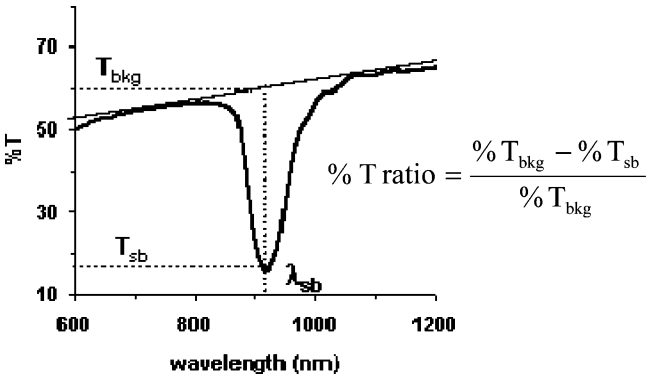

Figure 1. Attenuation by the stopband, %*T* ratio, expressed as the difference between the background transmission (T_{bkg}) and the minimum transmission (T_{sb}) determined at the central wavelength of the stopband.

Particle Characterization. The particles were imaged by using scanning electron microscopy (SEM, Hitachi S-5200 scanning electron microscope) at an accelerating voltage of 30 kV and a current of 10 mA. The latex dispersion was dried on a carbon-coated copper TEM grid and imaged under transmission mode. The average diameter and standard deviation of the microsphere sizes were obtained by analyzing the images using UTHSCSA Image Tool software.

The host colloid particles had a diameter of 295 nm and polydispersity (coefficient of variance, CV) of 2.3%. The guest colloid particles had diameters (polydispersity) of 319 (2.3%), 389 (2.3%), 271 (2.9%), and, 202 (2.8%) nm. The deviation in diameter, *x*, of the guest particles was expressed with respect to the host particles as

$$x = \frac{(\text{diameter of guest} - \text{diameter of host})}{(\text{diameter of host})}$$

Thus, guest particles with a size larger than the host beads had a positive deviation in particle size, that is, $x > 0$.

Preparation of Binary Dispersions. Four series of binary mixtures were prepared, with *x* of 8.0, 32, −8.0, and −32%. We mixed the dispersions of guest and host particles to obtain binary dispersions with particle number ratio, *y*, of $0.1 < y < 9.0\%$. The binary dispersions were then diluted with Milli-Q water to obtain 0.1 wt % colloid dispersions.

Colloid Crystal Growth. Glass substrates were cleaned in a piranha solution (1:3 H_2O_2/H_2SO_4) and rinsed thoroughly with Milli-Q water. Dried substrates were placed vertically into scintillation vials containing 20 mL of a 0.1 wt % binary colloid dispersion. The vials were covered with a 250 mL beaker and placed in an oven at 80 °C. Evaporation of water from the dispersion generally took ca. 48 h.

Optical Transmission of Colloid Crystals. Studies of optical transmission of CCs were measured on 4 ± 1 replicate samples

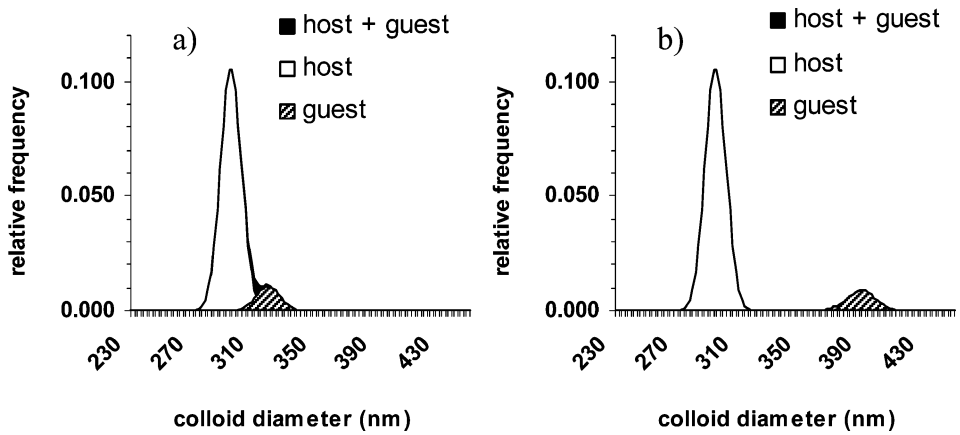

Figure 2. Size distribution for (a) $x = +8\%$ and (b) $x = +32\%$ for a concentration of guest particles of 10%. The size distributions of the host and guest particles were based on the mean particle diameter and standard deviations determined by SEM.

at four different points of each sample. A Varian Cary 5000 UV/VIS/NIR spectrophotometer was used for acquiring transmission spectra. An aperture 0.5 mm was placed behind the sample during transmission measurements. All measurements were made at normal incidence to the sample surface (parallel to a (111) crystallographic plane). In the spectral range of 650−750 nm, the spectra featured a dip in the transmission originating from the Bragg diffraction of the (111) plane of the colloid crystal.[37] To account for imperfect alignment of the samples, we used the relative transmission, that is, the transmission ratio (%T ratio), defined by the ratio of the difference in the background and minimum transmission of the stopband (%T_{bkg} and %$T_{sb,}$ respectively) to the background transmission (Figure 1).

We also examined the variation in the wavelength of the center of the stopband, λ_{sb}, and the change in the full width at half maximum, fwhm, of the stopband. Because the optical properties of the CCs depend on the number of crystal planes (N), we determined the thickness of the CCs in terms of the number of layers of colloid particles. The value of N was determined from Fabry−Perot fringes in the spectral range from 900 to 1800 nm, which originated from destructive interference from reflections from the front and back facets of the colloid crystal.[38] By approximating the effective refractive index, $n_{eff,}$ of the CC as $n_{eff} = (0.74n_{PMMA}^2 + 0.26n_{air}^2)^{1/2}$,[37] where n_{PMMA} and n_{air} are the refractive indices of PMMA and air (1.49 and 1.00, respectively), the thickness of the CC (expressed by the number of (111) planes, N) was

$$N = \frac{L}{d_{111}} = \frac{\lambda_1\lambda_2}{(\lambda_1 - \lambda_2)} \frac{1}{2\sqrt{2/3}n_{eff}D}$$

where L is

$$L = \frac{\lambda_1\lambda_2}{(\lambda_1 - \lambda_2)} \frac{1}{2n_{eff}}$$

and λ_1 and λ_2 are the wavelengths of two consecutive maxima in the interference fringe, D is the diameter of the colloid particle, and d_{111} is the interplanar distance of the (111) planes ($d_{111} = (^2/_3)^{1/2}D$).

Imaging of Colloid Crystals. The structure of the CCs was analyzed using a Hitachi S-570 scanning electron microscope (SEM) at an accelerated voltage of 15 kV and a working distance of 15 mm. The CCs were mounted onto an aluminum stub with carbon tape and coated with a thin layer of gold prior to SEM imaging. By using high scanning speeds, we ensured that the electron beam of the SEM did not alter the crystalline lattice of the sample.

Sphere Packing Algorithm. An algorithm based on simulated annealing provided a numerical model of CCs formed from particles with a binary size distribution. The algorithm sought the densest nonoverlapping arrangement of a collection of two populations of particles whose size distributions corresponded to those used in experiments. In the simulations, initially, the particles were placed at random positions above a single hexagonally packed "seed" layer. The energy of the system, E, was defined as the sum of three terms: (i) a one-dimensional downward potential, (ii) a short-range interparticle attraction, and (iii) a hard-sphere repulsion potential. The algorithm searched for the lowest-energy configuration by attempting random small movements of every particle. Movements that decreased the energy were always accepted, while those that increased the energy of the system were accepted with a probability $e^{-E/T}$, where T is the "temperature" of the system. This approach provided a certain freedom to the system and prevented it from being trapped in a local energy minimum. As time progressed, the energy decreased exponentially. Periodic boundary conditions were used in transverse directions, with the repetition cell large enough to accommodate 12 × 12 particles. The final arrays comprised 3024 particles, enough to fill 21 hexagonally packed layers. For each particle, 10^6 movements were attempted. In previous studies,[33] this algorithm produced ordered close-packed lattices from dispersions of identical spheres and close-to-realistic assemblies of polydispersed spheres. More details on the algoritm used can be found elsewhere.[33]

The optical transmittance of these arrays was computed with the well-established method of finite differences in the time domain.[39] The transmittance was calculated by launching a broadband wave pulse on one side of the array and computing the spectrum of the wave emerging normally on the other side of the array.

Results and Discussion

We conducted four series of experiments to examine the effect of the concentration and size of guest particles on the structure and the optical properties of colloid crystals. Prior to experiments, we ensured that the difference in size of the particles did not drive massive size segregation in the CCs for concentrations of guest particles up to ca. 9%.

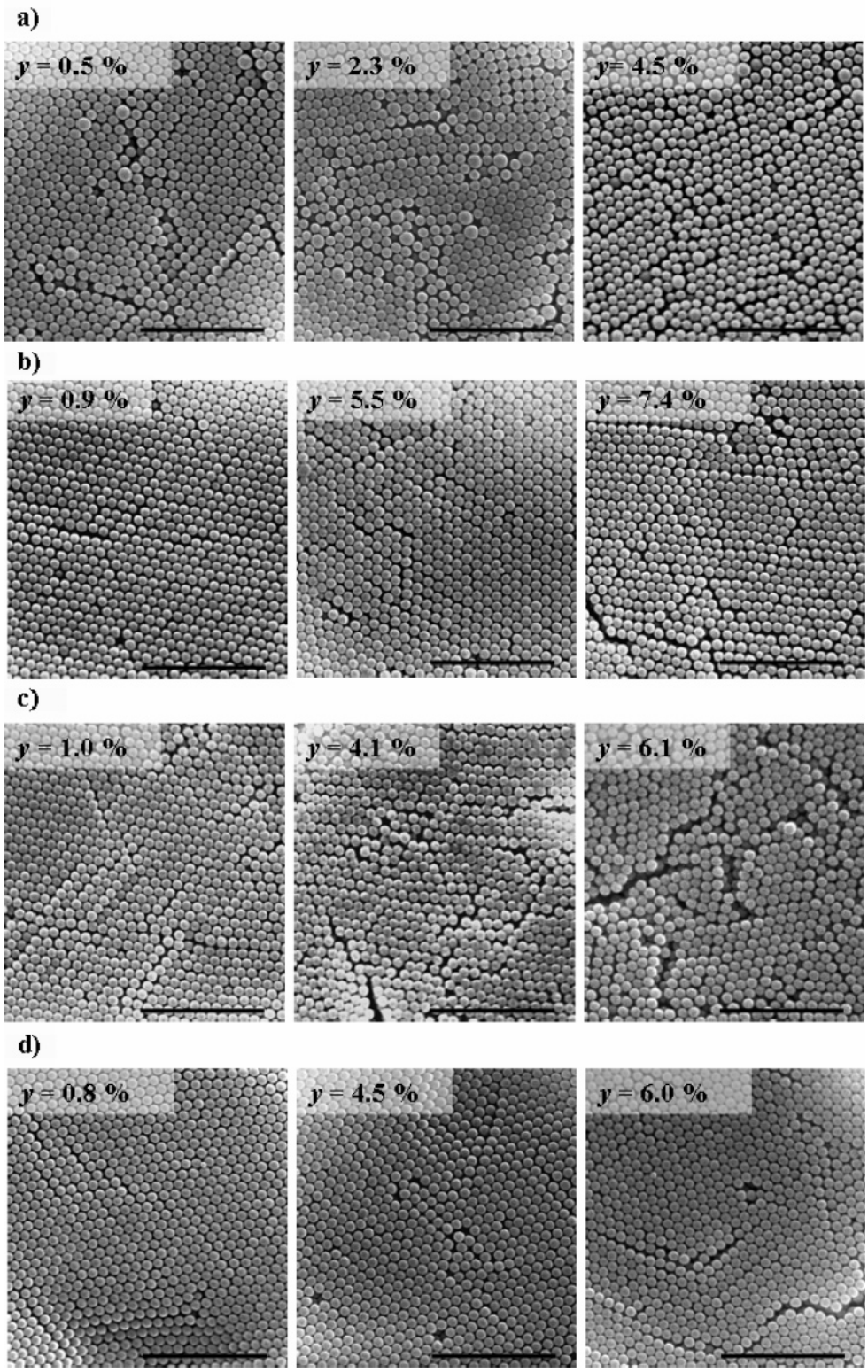

Figure 3. SEM images of CCs for series (a) +32%, (b) +8%, (c) −32%, and (d) −8%. The concentration of guest particles is expressed as the particle number density (y). The scale bar is 3.0 μm.

The difference in size between the guest and host particles, x, as defined in the Experimental Section, was −32, +32, +8, and −8%. Each population of colloid particles possessed a small intrinsic polydispersity of 2.3 < CV < 2.9%. For the $x = +8\%$ and $x = -8\%$ series, the difference in diameter between the host and guest microspheres was small enough that the overall particle size distribution was only slightly broadened (Figure 2a). For the $x = +32\%$ and $x = -32\%$ series, however, the large difference in diameter between the host and guest beads resulted in a bimodal size distribution (Figure 2b).

Structure of Guest−Host Colloid Crystals. Figure 3 shows typical SEM images of colloid crystals with different concentrations of guest particles. For all four series, the crystalline lattices appeared progressively more disordered as the concentration of guest particles increased. The rate at which the structural

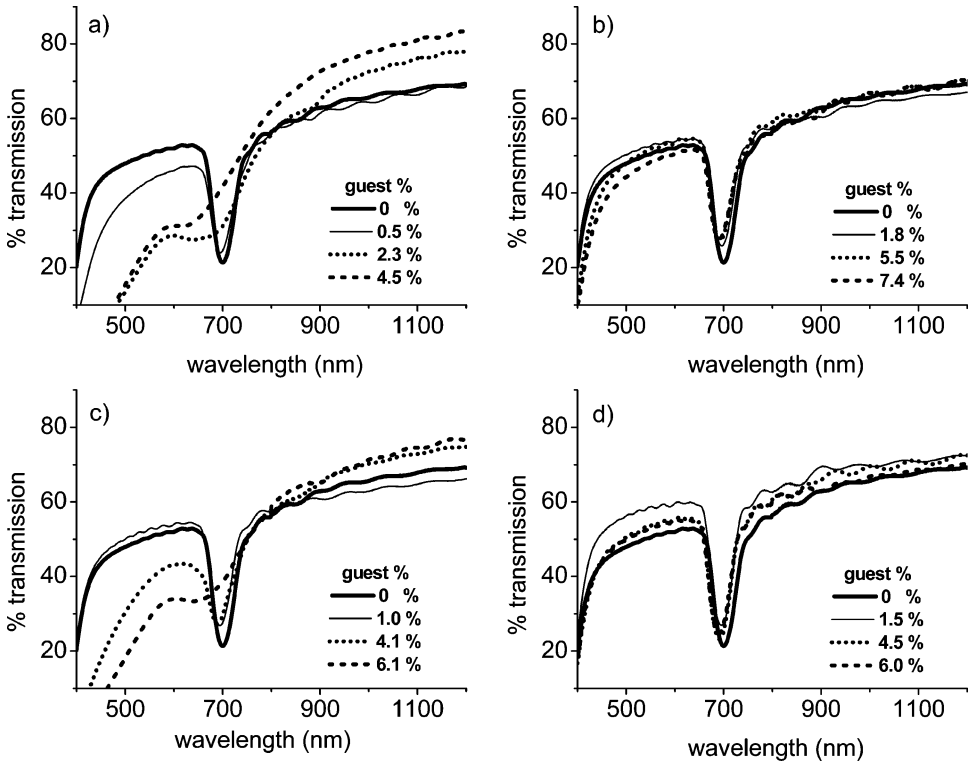

Figure 4. Transmission spectra of guest/host colloid crystals for series (a) +32%, (b) +8%, (c) −32%, and (d) −8%.

changes occurred depended on the size of the guest particles. For instance, in the +8% and −8% series, the presence of guest particles in concentrations as high as 6.0% had little impact on the lattice. This behavior contrasted with the CCs of the +32% and −32% series. In the case of the +32% series, the lattice was strongly disrupted by particles for concentrations as low as 0.5%, while for the −32% series, disruption was apparent at 4% of guest beads.

The images in Figure 3 also clearly demonstrate the different impact of large and small guest particles. The large guest beads ($x = +32\%$) intruded on neighboring lattice sites, producing defects. The defects accumulated with each guest particle and evolved into long-ranged disorder. Small guest particles ($x = -32\%$), at their low concentrations, did not intrude on neighboring sites, which largely preserved the lattice from disturbances. At higher concentrations of small guest particles, however, the guest beads modified the lattice and the CCs featured a more significant disruption.

Optical Properties of Guest−Host Colloid Crystals. Figure 4 shows representative optical transmission spectra measured for the colloid crystals of the same thickness, for different concentrations of guest microspheres. The transmission spectra of the +32, +8, −32, and −8% series featured similar trends with increasing concentrations of guest particles: an increasing transmission in the stopband, a broadening of the stopband, and a blue shift of the central wavelength of the stopband. The blue shift of the stopband likely originated from two effects: the decreasing background transmission at short wavelengths and the decrease in the effective refractive index, the latter imparted by the increased fraction of voids in disordered crystals (see SEM images, Figure 3). Another prominent feature of the transmission spectra was the large attenuation at wavelengths outside of the stopband (particularly, on the short wavelength side) observed for high concentrations of guest particles. We explain this effect as follows. At low fractions of guest particles, the main defects of the CCs were formed by cracks with sizes

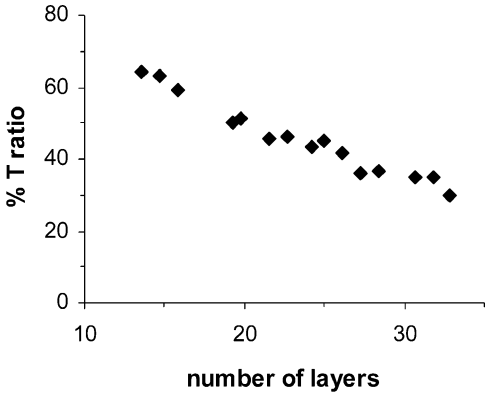

Figure 5. Variation in the %*T* ratio of the stopband of a colloid crystal in the absence of guest particles plotted as a function of the number of layers.

significantly larger than the wavelength of visible light.[21] With an increasing fraction of guest particles, the cracks decreased in size and much smaller defects, such as dislocations with sizes comparable to the wavelength of light, concurrently appeared. The scattering by these defects resembled Rayleigh scattering, thus decreasing the background transmission at shorter wavelengths.

Further investigation of the optical properties of CCs included comparison of the values of %*T* ratio, fwhm, and λ_{SB}. To account for the effect of the thickness of the CCs on the values of transmission, fwhm, and λ_{sb}, we first examined the variation of stopband features with the number of crystal planes, *N*, for crystals containing *no guest particles*. We found that for $19 < N < 24$, the fwhm and the λ_{sb} were independent of the number of crystal planes; however, the attenuation (the value of %*T* ratio) decreased with an increasing number of crystal planes (Figure 5). To account for this dependence, we used the normalized transmission, *T*′, obtained by dividing the %*T* ratio

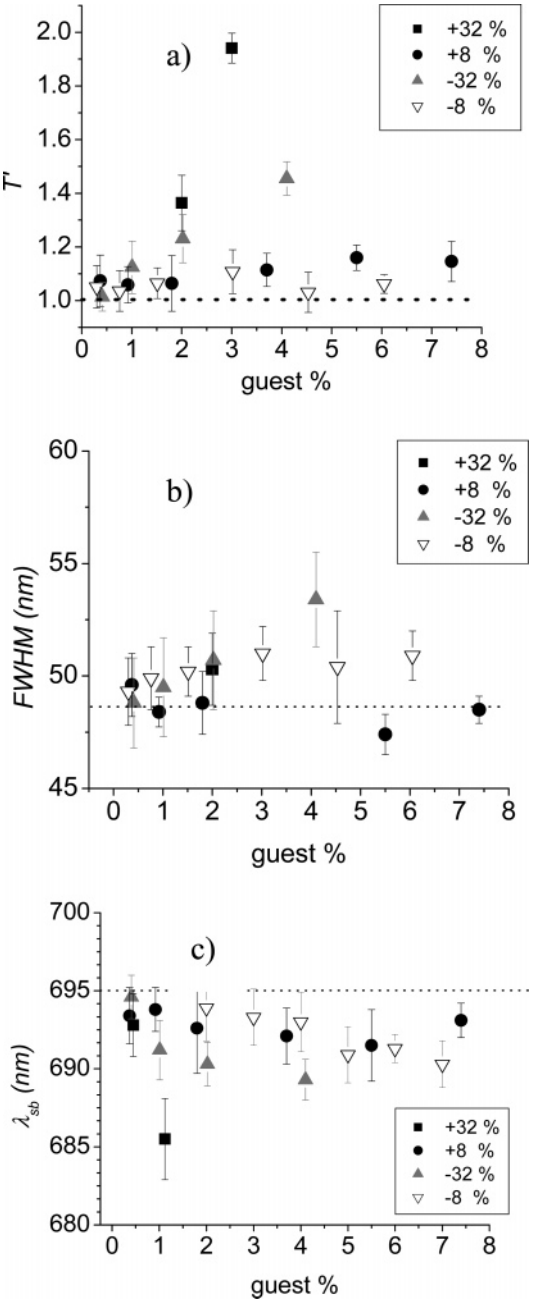

Figure 6. Variation in stopband properties of guest/host colloid crystals plotted as a function of the concentration of guest beads: T' (a), fwhm (b), and λ_{sb} (c).

for the guest/host CCs by the value of %T ratio for a colloid crystal of equal thickness containing *no guest particles*. In this approach, $T' = 1$ implies that the transmission in the stopband of the guest−host CC is equal to the transmission of a CC free of guest particles, whereas a $T' > 1$ implies that the attenuation for the guest−host CC is weaker than that for a guest-free CC.

In Figure 6, the normalized transmission, T', the central wavelength, λ_{sb}, and the fwhm of the stopband are plotted as a function of the concentration of guest particles. The horizontal dashed lines in Figure 6 represent the properties of the corresponding colloid crystal of similar thickness in the absence of guest particles. Figure 6 shows that (i) the attenuation remains strong for low concentrations of guest particles and (ii) at high concentration of guest microbeads the attenuation decreased, with concurrent broadening and blue shifting of the stopband. The extent to which the stopband was modified depended on the type of guest particles. Large guest particles ($x = +32\%$ and $x = +8\%$) and large absolute size deviations between the guest and host beads ($x = +32\%$ and $x = -32\%$ vs $x = +8\%$ and $x = -8\%$) caused more dramatic changes in the optical properties of CCs. In particular, the optical properties of the +32% series showed the highest sensitivity to the presence of guest particles, with the stopband degrading substantially at guest concentrations as low as 0.5%, while the optical properties of the −32% series showed a significantly decreased attenuation and broadened stopband at a concentration of guest particles of 4%. These concentrations, which produce significantly modified stopbands, correlated with the structural degradation of the corresponding guest−host CCs, as observed in the SEM images. We note that above a guest concentration of 4% and 0.5%, for the −32% +32% series, respectively, the values of T′, fwhm, and λ_{sb} were off-scale and the results were not included in the graphs.

In contrast, the colloid crystals of −8% series showed no appreciable change in optical properties for the entire range of concentrations of guest beads studied, while the +8% series featured small changes in the normalized transmission at guest concentrations of 5 ± 1%. The slight broadening in the size distribution produced by the guest particles of these series did not significantly impact the lattice structure and the optical properties of the crystal, in agreement with the corresponding SEM images.

Sphere Packing and Transmission Simulations. Figure 7 shows computer-rendered images of the cross-sections of particle arrays, which were generated by the simulated annealing algorithm.[33] Such simulations, in which the position of each particle is known, provide information that is complementary to the SEM imaging of the interior structure of the colloid crystals.

Figure 7e shows that even in the absence of guest particles, the lattice was not perfect: the intrinsic polydispersity of host particles (CV = 2.3%) was sufficiently large to introduce small disruption in the lattice. The impact of introducing guest particles in the arrays depended on the difference in size between the guest and host particles, which was in qualitative agreement with the experiments. For the series $x = +8\%$ or $x = -8\%$, the lattices with different concentrations of guest particles were similar in appearance, since the introduction of guest particles with small size differences did not significantly broaden the size distribution of the colloid system. In contrast, there was a clear impact on the lattice when the size difference was larger. As in experiments, the effect was different for the series $x = +32\%$ and $x = -32\%$. When the guest particles were smaller than the host particles ($x = -32\%$), the lattice accommodated a small number of guest particles by forming cage structures around them (thus showing self-healing properties). In the $x = +32\%$ series, the presence of guest particles transformed the lattice into a random-packed structure for concentrations of 1% and above, again in agreement with experimental results.

Figure 8 shows the simulated optical properties of the arrays. By contrast with experimental spectra in which the transmission was averaged over a large area of the crystal, the simulated spectra appeared noisy because of the limited lateral size of the arrays. As in the experimental transmission spectra, the stopband in the simulated spectra emerged as a sharp dip in the transmission.

When guest particles were introduced in the arrays, the changes in the spectra correlated with the experimental results. The introduction of guest particles of the +8% and −8% series did not affect the spectra significantly, since the lattice did not

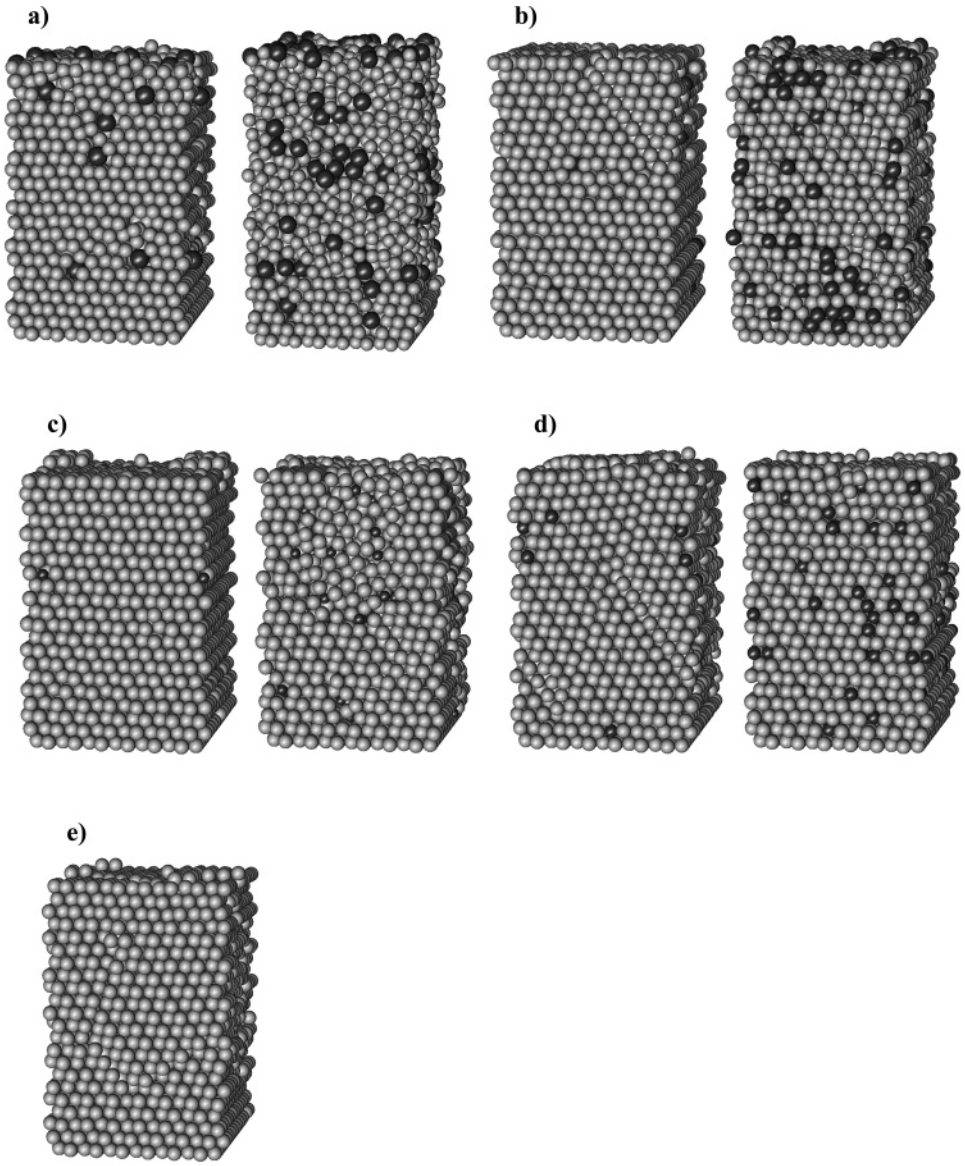

Figure 7. Computer-rendered images of the simulated guest/host CCs of series (a) +32%, (b) +8%, (c) −32%, (d) −8%, and (e) guest-free CC. In parts a−d, the left image possesses 1% of the guest particles and the right image possesses 8% of the guest particles.

undergo noticeable changes. For the simulation of the $x = +32\%$ or $x = -32\%$ series, the attenuation in the stopband gradually decreased. In addition, with increasing concentration of guest particles, the stopband slightly blueshifted and became wider. Another less obvious change in the spectra with increasing guest concentration was the reduced transmission outside of the stopband, which signified that the Rayleigh-type scattering depended on the extent of ordering of the array. We note that, because the simulation did not include the effect of reflections on both faces of the glass substrates, the maximum transmission approached 100% in the simulations, whereas in experiments it never exceeded 90%.

In Figure 9, we compared the simulated and measured experimental variation in the maximum attenuation of the stopband with the concentration of guest particles. Overall, the trends observed in simulations and experiments were similar. In parts a and c of Figure 9, the experimental and simulated attenuation of the $x = +32\%$ and $x = -32\%$ series underwent the same rapid decrease at very low concentrations of guest particles: for the concentration of 2% in the $x = +32\%$ series and 4% in the $x = -32\%$ series. Parts b and d of Figure 9 show that for the concentration of guest particles below 2% the experimental and simulated attenuation remained close to constant for the + 8% and −8% series. In Figure 9d, the simulated normalized transmission data for the −8% colloid crystals had a slightly better quality ($T' < 1$) than the host-only crystal. This effect can be traced back to a slightly decreased simulated transmission at the bottom of the stopband for the same background transmission (Figure 8).

Close examination of the simulated arrays in Figure 7d revealed that the presence of guest particles whose diameter only marginally deviated from the host diameter helped the lattice accommodate the collection of particles with the given size distribution. This feature was not observed in the experiments, in which a minor excess of smaller particles decreased the transmission in comparison to host-only crystals. At the moment, it is not clear whether this is an artifact of the model or this effect truly takes place in real colloid crystals but is too small to be measured. Finally, the decrease in T' at 1% guest concentration for the +32% and −32% (parts a and c of Figure 9) can be attributed to the stochastic nature of the model and the limited lateral size of the arrays in simulations.

We take the general agreement between experimental and simulation results as a confirmation that the arrangement of

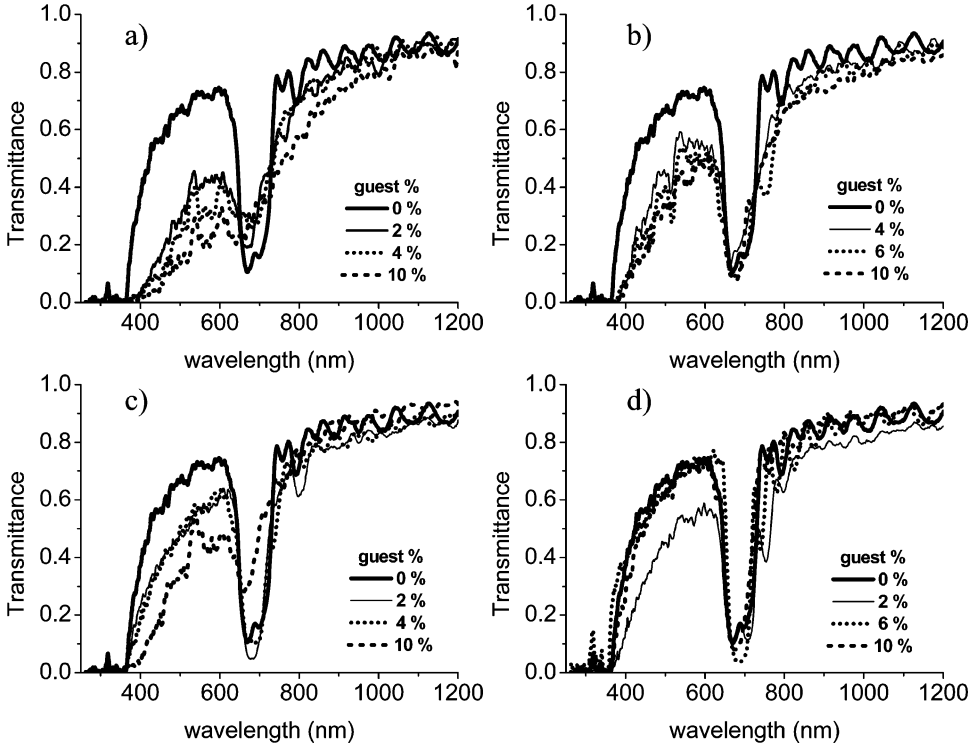

Figure 8. Simulated transmission spectra of the guest/host CCs at different concentrations of guest particles for the series (a) +32%, (b) +8%, (c) −32%, and (d) −8%.

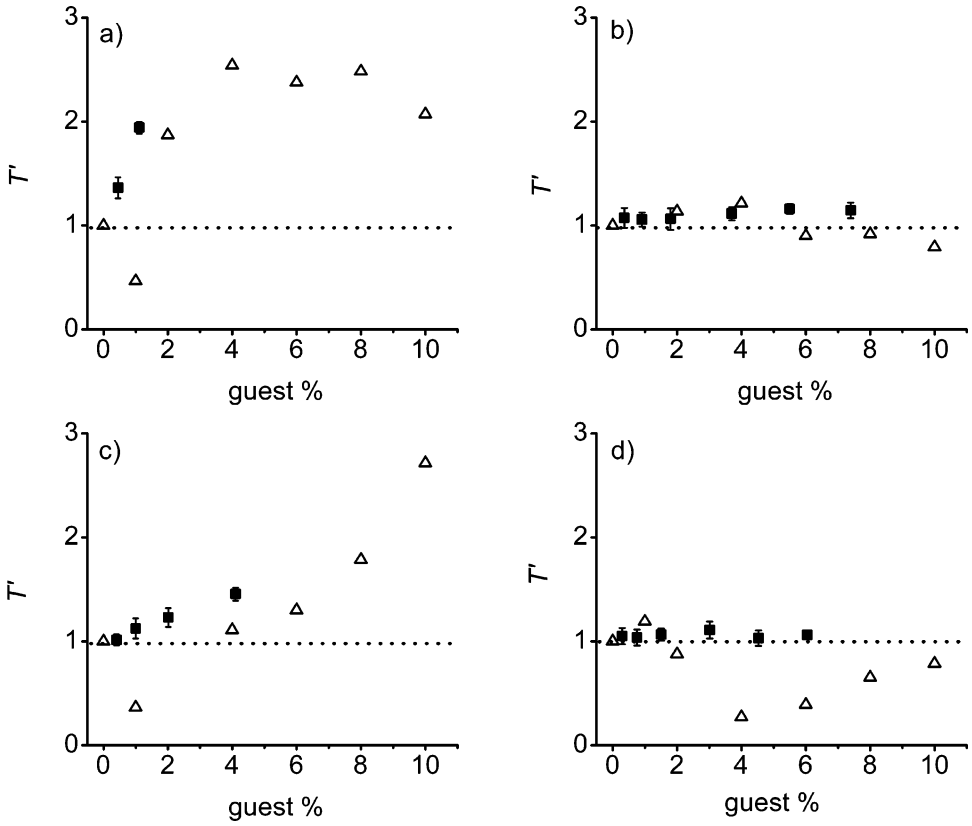

Figure 9. Comparison of simulated (△) and experimental (■) normalized transmission for series: (a) $x = +32\%$, (b) $x = +8$ %, (c) $x = -32\%$, and (d) $x = -8\%$.

particles in the simulated arrays are representative of those in real colloid crystals. The model presented here can therefore be used to study the impact of polydispersity on the optical properties of CCs.

Conclusion

The structure and optical properties of guest/host colloid crystals were examined experimentally (by SEM imaging and

optical diffraction spectroscopy, respectively) and by simulating crystallization of the collection of particles. The results of SEM imaging of the structure of CCs show the lattices were only marginally affected by the presence of guest particles with sizes on the fringes of the host size distribution, which, in turn, did not significantly modify the optical properties of the CCs. In contrast, guest particles with large size deviations from host microspheres showed two different types of behavior.

For *small guest particles*, a high extent of order was preserved at a low concentration of guest particles but collapsed into a random-packed structure at a high concentration of guest particles. Both the simulations and SEM imaging revealed that at low guest concentrations, the host particles formed a cage structure around smaller guest particles without ensuing changes in the lattice. At higher concentrations of smaller guest particles, however, a collapse of the cage structures disrupted the lattice and degraded the optical properties.

In the case of *larger guest particles*, the particles infringed on the neighboring lattice sites, displacing the host colloids from the lattice sites and thus causing long-range disruptions at very low guest concentrations. Simulations of the formation of colloid arrays from particles with bimodal distribution helped to understand how the lattice accommodates guest particles of different sizes and in certain concentrations. The results of this work highlight the importance of controlling the size distribution of colloid particles before their self-assembly into colloid crystals.

References and Notes

(1) Chutinan, A.; Noda, S. *Science* **1999**, *282*, 274−276.

(2) Pan, G.; Kesavamoorthy, R.; Asher, S. A. *Phys. Rev. Lett.* **1997**, *78*, 3860−3863.

(3) Shimoda, Y.; Ozaki, M.; Yoshino, K. *Appl. Phys. Lett,* **2001**, *79*, 3627−3629.

(4) Mayoral, R.; Requena, J.; Moya, J. S.; López, C.; Cintas, A.; Míguez, H.; Meseguer, F.; Vázquez, L.; Holgado, M.; Blanco, A. *Adv. Mater.* **1997**, *9*, 257−258.

(5) Jiang, P.; McFarland, M. J. *J. Am. Chem. Soc.* **2004**, *126*, 13778−13786.

(6) Van Blaaderen, A.; Ruel, R.; Wiltzius, P. *Nature* **1997**, *385*, 321−324.

(7) Allard, M.; Sargent, E. H.; Lewis, P. C.; Kumacheva, E. *Adv. Mater.* **2004**, *16*, 1360−1364.

(8) Lu, Y.; Yin, Y.; Gates, B.; Xia, Y. *Langmuir* **2001**, *17*, 6344−6350.

(9) Park, S. H.; Qin, D.; Xia, Y. *Adv. Mater.* **1998**, *10*, 1045−1049.

(10) Míguez, H.; Yang, S. M.; Ozin, G. A. *Appl. Phys. Lett.* **2002**, *81*, 2493−2495.

(11) Kumacheva, E.; Golding, R. K.; Allard, M.; Sargent, E. H. *Adv. Mater.* **2002**, *14*, 221−224.

(12) Vickreva, O.; Kalinina, O.; Kumacheva, E. *Adv. Mater.* **2000**, *12*, 110−112.

(13) Trau, M.; Saville, D. A.; Aksay, I. A. *Science* **1996**, *272*, 706−709.

(14) Rogach, A. L.; Kotov, N. A.; Koktysh, D. S.; Ostrander, J. W.; Ragoisha, G. A. *Chem. Mater.* **2000**, *12*, 2721−2726.

(15) Helseth, L. E.; Wen, H. Z.; Hansen, R. W.; Johansen, T. H.; Heinig, P.; Fischer, T. M. *Langmuir* **2004**, *20*, 7323−7332.

(16) Jiang, P.; Bertone, J. F.; Hwang, K. S.; Colvin, V. L. *Chem. Mater.* **1999**, *11*, 2132−2140.

(17) Denkok, N. D.; Velev, O. D.; Kralchevsky, P. A.; Ivanov, I. B.; Yoshimuri, H.; Nagayama, K. *Langmuir* **1992**, *8*, 3183−3190.

(18) Cong, H.; Cao, W. *Langmuir* **2003**, *19*, 8177−8181.

(19) Ye, Y.-H.; LeBlanc, F.; Hache, A.; Truong, V. V. *Appl. Phys. Lett.* **2001**, *78*, 52−54.

(20) Rodner, S. C.; Wedin, P.; Bergström, L. *Langmuir* **2002**, *18*, 9327−9333.

(21) McLachlan, M. A.; Johnson, N. P.; De La Rue, R. M.; McComb, D. W. *J. Mater. Chem.* **2004**, *14*, 144−150.

(22) Dimitrov, A. S.; Nagayama, K. *Langmuir* **1996**, *12*, 1303−1311.

(23) Rengarajan, R.; Mittleman, D.; Rich, C.; Colvin, V. *Phys. Rev. E* **2005**, *71*, 16615.

(24) Gates, B.; Xia, Y. *Appl. Phys. Lett.* **2001**, *78*, 3178−3180.

(25) Vlasov, A.; Kaliteevski, M. A.; Nikolaev, V. V. *Phys. Rev. B* **1999**, *60*, 1555−1562.

(26) Li, Z.-Y.; Zhang, Z.-Q. *Phys. Rev. B* **2000**, *62*, 1516−1519.

(27) Kaliteevski, M.; Manzanares Martinez, J.; Cassagne, D.; Albert, J. P. *Phys. Status Solidi* **2003**, *195*, 612−617.

(28) Allard, M.; Sargent, E. H.; Kumacheva, E.; Kalinina, O. *Opt. Quantum Electron.* **2002**, *34*, 27−36.

(29) Rojas-Ochoa, L. F.; Mendez-Alcaraz, J. M.; Sáenz, J. J.; Schurtenberger, P.; Scheffold, F. *Phys. Rev. Lett*, **2004**, *93*, 73903.

(30) Solovyev, V. G.; Romanov, S. G.; Chigrin, D. N.; Sotomayor Torres, C. M. *Synth. Met.* **2003**, *139*, 601−604.

(31) Ballato, J.; Dimaio, J.; James, A.; Gulliver, E. *Appl. Phys. Lett.* **1999**, *75*, 1497-

(32) Kaliteevski, M. A.; Martinez, J. M.; Cassagne, D.; Albert, J. P. *Phys. Rev. B* **2002**, *66*, 113101.

(33) Allard, M.; Sargent, E. H. *Appl. Phys. Lett.* **2004**, *85*, 5887−5889.

(34) O'Callaghan, K. J.; Paine, A. J.; Rudin, A. *J. Appl. Polym. Sci.* **1995**, *58*, 2047−2055.

(35) Stöber, W.; Fink, A.; Bohn, E. *J. Colloid Interface Sci.* **1968**, *26*, 62−69.

(36) Kalinina, O.; Kumacheva, E. *Macromolecules*, **1999**, *32*, 4122−4129.

(37) Míguez, H.; López, C.; Meseguer, F.; Blanco, A.; Vázquez, L.; Mayoral, R. *Appl. Phys. Lett.* **1997**, *9*, 1148−1150.

(38) Reculusa, S.; Massé, P.; Ravaine, S. *Colloid Interface Sci.* **2004**, *279*, 471−478.

(39) Taflove, A.; Hagness, S. C. *Computational Electrodynamics: The Finite-Difference Time-Domain Method*, 2nd ed.; Artech House: Boston, MA, 2000; pp 1−852.